

Performance analysis of an in-built N^+ pocket electrically doped TFET biosensor for biomedical applications

Chan Shan(单婵), Qian-nan Wang(王倩楠), and Ying Liu(刘赢)
Citation: Chin. Phys. B, 2026, 35 (**2**): 028703. DOI: 10.1088/1674-1056/adecfa
http://cpb.iphy.ac.cn; http://iopscience.iop.org/cpb

What follows is a list of articles you may be interested in

Impacts of aging on the entrainment capability of the mammalian circadian system

Ji Zhou(周吉) and Ying Li(李莹)
Chin. Phys. B, 2025, 34 (**7**): 078701. DOI: 10.1088/1674-1056/adce92

Terahertz toroidal dipole metamaterial sensors for detection of aflatoxin B1

Jianwei Xu(徐建伟), Shoujian Ouyang(欧阳收剑), Shouxin Duan(段守鑫), Liner Zou(邹林儿), Danni Ye(叶丹妮), Sijia Yang(杨思嘉), and Xiaohua Deng(邓晓华)
Chin. Phys. B, 2024, 33 (**3**): 038701. DOI: 10.1088/1674-1056/acef02

Effect of short-term plasticity on working memory

Fan Yang(杨帆) and Feng Liu(刘锋)
Chin. Phys. B, 2023, 32 (**11**): 118706. DOI: 10.1088/1674-1056/acf03a

Free running period affected by network structures of suprachiasmatic nucleus neurons exposed to constant light

Jian Zhou(周建), Changgui Gu(顾长贵), Yuxuan Song(宋雨轩), and Yan Xu(许艳)
Chin. Phys. B, 2023, 32 (**9**): 098701. DOI: 10.1088/1674-1056/acd7ce

Thermally enhanced photoluminescence and temperature sensing properties of $Sc_2W_3O_{12}:Eu^{3+}$ phosphors

Yu-De Niu(牛毓德), Yu-Zhen Wang(汪玉珍), Kai-Ming Zhu(朱凯明), Wang-Gui Ye(叶王贵), Zhe Feng(冯喆), Hui Liu(柳挥), Xin Yi(易鑫), Yi-Huan Wang(王怡欢), and Xuan-Yi Yuan(袁轩一)
Chin. Phys. B, 2023, 32 (**2**): 028703. DOI: 10.1088/1674-1056/ac70b8

Performance analysis of an in-built N^+ pocket electrically doped TFET biosensor for biomedical applications

Chan Shan(单婵)[1], Qian-nan Wang(王倩楠)[1], and Ying Liu(刘赢)[2,3,†]

[1] *School of Ocean Information Engineering, Jimei University, Xiamen* 361021, *China*
[2] *Faculty of Data Science and Information Technology, INTI International University, Negeri Sembilan*, 71800, *Malaysia*
[3] *School of Software, Quanzhou University of Information Engineering, Quanzhou* 362008, *China*

(Received 30 April 2025; revised manuscript received 12 June 2025; accepted manuscript online 8 July 2025)

An in-built N^+ pocket electrically doped tunnel field-effect transistor (ED-TFET)-based biosensor has been reported for the first time. The proposed device begins with a PN junction structure with a control gate (CG) and two polarity gates (PG1 and PG2). Utilizing the polarity bias concept, a narrow N^+ pocket is formed between the source and channel without the need for additional doping steps, achieved through biasing PG1 and PG2 at −1.2 V and 1.2 V, respectively. This method not only addresses issues related to doping control but also eliminates constraints associated with thermal budgets and simplifies the fabrication process compared to traditional TFETs. To facilitate biomolecule sensing within the device, a nanogap cavity is formed in the gate dielectric by selectively etching a section of the polarity gate dielectric layer toward the source side. The investigation into the presence of neutral and charged molecules within the cavities has been conducted by examining variations in the electrical properties of the proposed biosensor. Key characteristics assessed include drain current, energy band, and electric field distribution. The performance of the biosensor is measured using various metrics such as drain current (I_{DS}), subthreshold swing (SS), threshold voltage (V_{TH}), drain current ratio (I_{ON}/I_{OFF}). The proposed in-built N^+ pocket ED-TFET-based biosensor reaches a peak sensitivity of 1.08×10^{13} for a neutral biomolecule in a completely filled nanogap with a dielectric constant of 12. Additionally, the effects of cavity geometry and different fill factors (FFs) on sensitivity are studied.

Keywords: electrically doped, label-free biosensors, PNPN tunnel field-effect transistors (TFETs), sensitivity

PACS: 87.85.fk, 85.30.Tv, 85.30.De, 85.30.Mn

DOI: 10.1088/1674-1056/adecfa **CSTR:** 32038.14.CPB.adecfa

1. Introduction

Biosensors are essential in our rapidly evolving technological landscape, with their market anticipated to expand consistently in the years ahead. These innovative devices find widespread application in numerous areas, such as biological molecule research, food product testing, environmental monitoring, forensic science, and pharmaceutical development.[1] Key design factors for biosensors include sensitivity, selectivity, and rapid detection times. As a result, field-effect transistor (FET)-based biosensors have surfaced as a budget-friendly alternative to costly laboratory sensors, providing label-free detection of biomolecules.[2–4] This approach not only delivers precise results without affecting the inherent properties of the biomolecules but also brings several additional benefits. These advantages include compatibility with CMOS technology regarding size, the ability to sense a broad spectrum of biological species, high sensitivity, low power consumption, and the possibility of being integrated onto a single chip.[5,6] Despite their compact size and low cost, the scaling of FET-based devices encounters several challenges, including short-channel effects (SCEs), OFF-state conduction, subthreshold roll-off, drain-induced barrier lowering (DIBL), and subthreshold swing (SS) greater than 60 mV/dec. These issues can negatively impact the performance of FET-based biosensors. To tackle the challenges mentioned above, various tunnel-field-effect-transistor (TFET)-based biosensors have been proposed. These biosensors demonstrate a steep subthreshold swing, low power consumption, rapid response times, and high sensitivity.[7–11]

In addition to the advantages mentioned, TFETs also face certain limitations, such as low ON-current and ambipolar conduction. Numerous studies have been conducted by researchers to address the issue of low current in TFETs. Some of these studies have explored the use of dual-material gate structures with double gate configurations through gate material engineering.[12] Additionally, various TFET device architectures have been proposed, including gate-all-around, Z-shaped gate, L-shaped gate, and T-shaped gate, employing structural engineering techniques.[13–15] Meanwhile, the source-pocket (PNPN) TFET features a narrow, highly doped N+ pocket layer located between the source and the channel, which improves the overall performance of the traditional P–I–N TFET design.[16,17] However, creating the narrow, highly doped N^+ pocket requires a steep doping concentration gradient, leading to several challenges such as greater fabrication

†Corresponding author. E-mail: liuying@foxmail.com

© 2026 Chinese Physical Society and IOP Publishing Ltd. All rights, including for text and data mining, AI training, and similar technologies, are reserved.

complexity, random dopant fluctuations (RDFs), an increased thermal budget, and costly annealing processes. These factors pose significant concerns for TFET-based biosensors.

Utilizing the polarity bias concept, we have recently introduced a theoretical device design for an electrically doped (ED) TFET that features an in-built N^+ pocket.[18] Using electrical doping instead of traditional doping methods removes the need for abrupt doping profiles at junctions, reduces the thermal budget, and avoids the ion implantation process during device fabrication. As noted in Ref. [19] the OFF-state current in ED-TFET is significantly lower than that of conventional TFETs. This reduction is attributed to the lightly doped silicon film and the lack of P–N junctions in thermal equilibrium. Furthermore, the proposed ED-TFET offers the potential for a much steeper subthreshold slope compared to conventional TFETs. In our earlier research, this in-built N^+ pocket ED-TFET was shown to effectively tackle the challenges of low ON-current, fabrication complexity, and RDFs commonly associated with traditional TFETs. Consequently, this manuscript explores the use of in-built N^+ pocket ED-TFET-based biosensors for biomolecule detection. Furthermore, a nanogap cavity is created within the oxide of the source region adjacent to the in-built N^+ pocket rather than in the control gate oxide region. The sensing mechanism of the proposed biosensors relies on the modulation of oxide capacitance caused by the immobilization of biomolecules within the nanocavity, which exhibit varying dielectric constants (k values) and interfacial charge densities (ρ values). In the simulation, the cavity is designed with an oxide layer material that has adjustable electrical properties (k and ρ values) to align with those of the desired biomolecules. By methodically modifying these parameters, a comprehensive analysis of the electrical performance trends of the proposed biosensor is conducted.

The main objective of the proposed device is to facilitate label-free detection of biological molecules, such as uricase, keratin, biotin, streptavidin, and more. A comprehensive analysis of the in-built N^+ pocket ED-TFET's performance has been conducted, examining various biosensing parameters, including electric field, energy band diagram, tunneling current, subthreshold slope, I_{ON}/I_{OFF} ratio, and threshold voltage.

This article is structured as follows: Section 2 covers the simulation parameters of the proposed device and fabrication steps. Section 3 presents the results along with a detailed discussion of the sensitivity analysis. Lastly, Section 4 summarizes our simulation study, highlighting the key findings.

2. Simulation parameters and fabrication process

Figure 1 illustrates the cross-sectional view of the in-built N^+ pocket ED-TFET biosensor, which features an integrated nanocavity within the oxide of the source region. The design parameters and dimensions used in this study are presented in Table 1. An in-built N^+ pocket electrically doped TFET is introduced by utilizing the polarity bias concept.[20] To create the N^+ drain and P^+ source regions within the device, suitable biases are applied to the polarity gate terminals, with V_{PG1} set at -1.2 V and V_{PG2} at 1.2 V, respectively. Beginning with a PN junction structure, two polarity gate electrodes are positioned on the source and drain sides of the device to form the PNPN TFET configuration. This arrangement allows for the creation of a narrow N^+ pocket within the device without requiring additional doping steps, thereby reducing manufacturing complexity. The work functions for polarity gate 1 (PG1) and polarity gate 2 (PG2) are 5.93 eV and 3.9 eV, respectively, corresponding to selenium (Se) and hafnium (Hf). For the control gate (CG) contact, the work function is 4.3 eV, which corresponds to ruthenium (Ru). Nickel silicide (NiSi), with a potential barrier of 0.45 eV, has been employed for the drain and source contacts.[19] NiSi possesses a low Schottky barrier height (SBH), which leads to a high density of charge carriers at its edges, thus enhancing the ON current. Additionally, simulations have shown that the incorporation of the in-built N^+ pocket provides a greater drive current and a steeper average subthreshold slope (SS) compared to traditional ED-TFETs.[21] The performance of the proposed biosensor benefits from the stacking of SiO_2 and HfO_2 oxides in the source region. Regarding the dimensions of the biomolecules, the cavity's length and width are set to 25 nm and 15 nm, respectively. The biomolecules targeted in this simulation — Biotin, APTES, Ferrocytochrome c, Keratin, and Gelatin — exhibit dielectric constants that vary between 2.63 and 12, as detailed in Table 2. In the absence of biomolecular occupancy within the nanocavity, there is a baseline dielectric constant of unity ($k = 1$), which corresponds to the permittivity of vacuum. The impact of biomolecular charges is examined at the SiO_2–insulator interface, with charge densities (ρ) defined based on recognized values for DNA.[22–26]

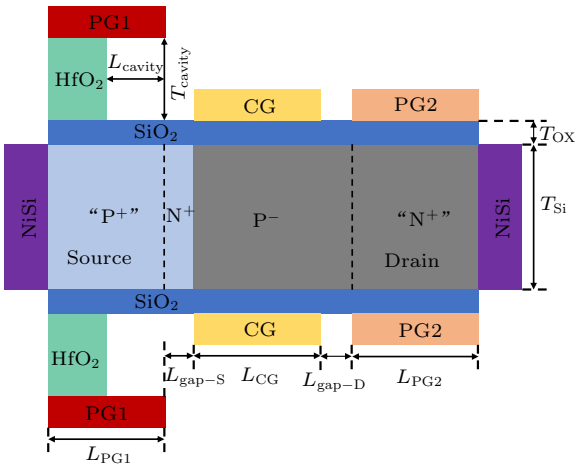


Fig. 1. Cross-sectional view of the in-built N^+ pocket ED-TFET biosensor.

Table 1. Simulation parameters and dimensions of the in-built N^+ pocket ED-TFET biosensor.

Design parameters	Symbol	Value
Silicon layer thickness	T_{Si}	10 nm
Source doping	N_S	4×10^{19} cm^{-3}
Body doping	N_B	1×10^{17} cm^{-3}
Length of CG/PG1/PG2	$L_{CG/PG1/PG2}$	50 nm
SiO_2 thickness	T_{ox}	1 nm
HfO_2 thickness	T_{HfO_2}	15 nm
Nanocavity length	L_{cavity}	25 nm
Nanocavity thickness	T_{cavity}	15 nm
CG workfunction	φ_{CG}	4.3 eV
PG1 workfunction	φ_{PG1}	5.93 eV
PG2 workfuction	φ_{PG2}	3.9 eV
PG2/PG1 voltage	$V_{PG2/PG1}$	±1.2 V
Source–gate/Drain–gate gap	L_{gap-S}/L_{gap-D}	5 nm

Table 2. Electrical properties for biomolecules.

Biomolecules	Dielectric constant (k)	Type
Biotin	2.63	neutral
APTES	3.57	neutral
Ferrocytochrome c	4.7	neutral
Keratin	8	neutral
Gelatin	12	nuutral
DNA	1-64	charged

Figure 2 depicts the fabrication steps for the proposed in-built N^+ pocket ED-TFET biosensor. These processes align with those previously documented in the referenced literature and are fully compatible with existing CMOS technology.[27–29] As shown in Fig. 2(a), the fabrication process for the proposed in-built N^+ pocket ED-TFET biosensor begins with a high-quality P-type monocrystalline silicon substrate, with a doping concentration of 1×10^{17} cm^{-3}. This ensures a uniform and defect-free crystalline structure, which is crucial for consistent device performance. Two distinct wafers undergo similar processing steps before they are ultimately bonded together. Each starting wafer resembles a silicon-on-insulator (SOI) wafer featuring a 5-nm-thick silicon layer. The wafer is subjected to Arsenic ion implantation for N^+ doping, while the portion of the wafer under the resist mask remains initial P-type doping, as illustrated in Fig. 2(b). After this, the resist mask is stripped away. In the subsequent step, illustrated in Fig. 2(c), a silicon dioxide (SiO_2) layer is grown on the P-type doping side of the silicon layer through oxidation processes, achieving a thickness of 1 nm, followed by the deposition of metal-1 with a work function of 3.9 eV. Following this, a second oxidation step and the deposition of metal-2, which has a work function of 4.3 eV, are carried out using similar processing techniques. As seen in Fig. 2(d), masking and selective etching techniques are employed to define CG and PG2. The next step involves depositing another 1-nm-thick SiO_2 layer, followed by the deposition of a hafnium oxide (HfO_2) layer through atomic layer deposition (ALD),[30] and then metal-3, which has a work function of 5.93 eV, is deposited through a metallization process, as depicted in Fig. 2(e).

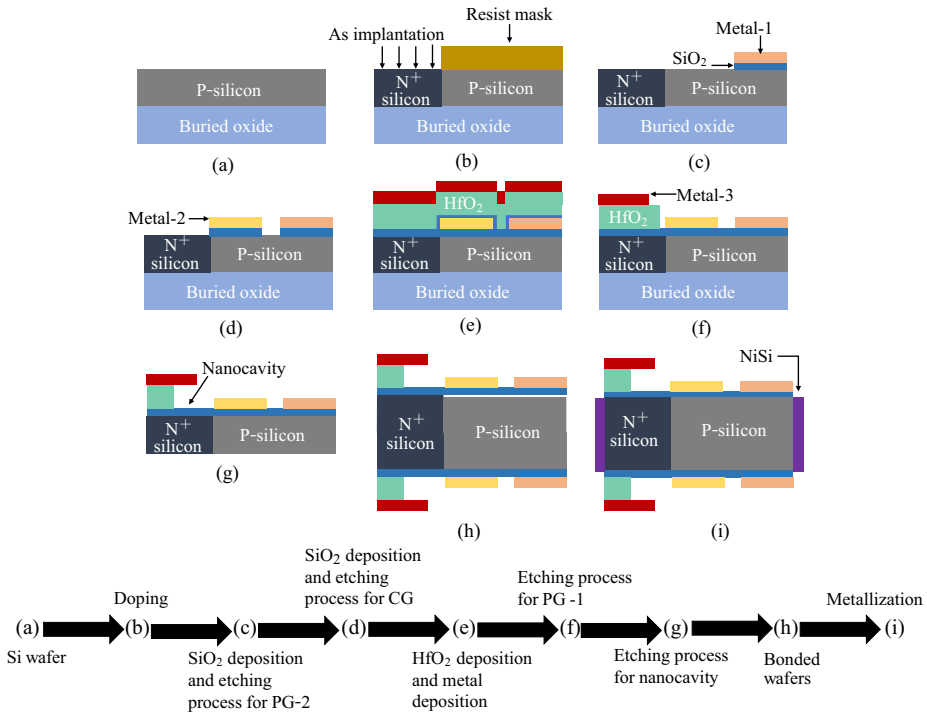


Fig. 2. Fabrication process for the in-built N^+ pocket ED-TFET biosensor.

Following this, figure 2(f) illustrates the selective etching required to form PG1. A nanocavity is created in the oxide region of PG1 using the neutral-beam-assisted atomic layer etching (NBALE) technique,[31] with the buried oxide layer subsequently etched away. The final structure is completed by bonding the two processed wafers together, as shown in Fig. 2(h).

The drain and source contacts are formed using NiSi, which is deposited via e-beam evaporation without the need for annealing. Any unreacted nickel is subsequently eliminated through selective wet etching using a hot piranha solution. The cross-sectional view of the completed in-built N^+ pocket ED-TFET biosensor is presented in Fig. 2(i).

All simulations were conducted using the Silvaco Atlas device simulation tool, version 5.19.20.R.[32] To account for mobility degradation due to electric fields, we implemented the Lombardi mobility model in our simulations. Additionally, we incorporated the Shockley–Read–Hall (SRH) recombination model and utilized Fermi–Dirac statistics to enhance the accuracy of carrier statistics. For devices operating at high doping concentrations, the band-gap narrowing (BGN) model was applied. It is important to note that quantum mechanical effects were not considered when the thickness of the silicon (T_{Si}) was greater than 7 nm.[33] Since T_{Si} was designed to be 10 nm, quantum mechanical effects were excluded from our simulations. To account for tunneling in the lateral direction, the non-local band-to-band tunneling (BTBT) model was employed. For these simulations, a fine mesh was utilized in the regions where tunneling occurs, allowing for a precise representation of tunneling effects.

The transfer characteristics of an experimentally fabricated N-TFET device were utilized to validate our simulated model and simulation approach. For the purpose of this validation, the dimensions, materials, and other properties of the simulated device were assumed to be identical to those of the fabricated N-TFET device. As shown in Fig. 3, the transfer characteristics of both the experimentally fabricated device and the simulated device are presented.[34]

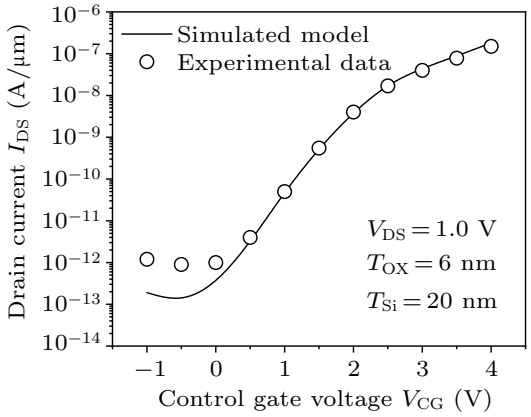


Fig. 3. Calibration of the simulated model with the experimental data.[34]

The results reveal a strong correlation between the two sets of characteristics, indicating that the simulation environment we have established accurately represents the behavior of the real device. This validation provides confidence in the reliability of our simulation model for predicting the performance of the N-TFET devices under study.

3. Results and discussion

In this section, we investigate the effects of neutral biological molecules with different k values in the cavity region on the electrical properties of the device. However, in the presence of charged biomolecules, we consider the fixed charge at the Si–SiO_2 interface. As reported in reference,[35] the effective capacitance at the source of the biosensor is a series combination of the capacitance of the biomolecular layer and the oxide layer. This can be expressed using the following equation:

$$\frac{1}{C_s} = \frac{1}{C_{Bio}} + \frac{1}{C_{ox}} = \frac{t_{Bio}}{k_{Bio}\varepsilon_{Bio}} + \frac{t_{ox}}{k_{ox}\varepsilon_{ox}}, \tag{1}$$

where C_{Bio}, k_{Bio}, and t_{Bio} denote the capacitance, dielectric constant, and thickness of the biomolecule layer, while C_{ox}, k_{ox}, and t_{ox} represent the capacitance, dielectric constant, and thickness of the oxide layer, respectively. C_s signifies the biosensor's effective capacitance at the source. It is noteworthy that equation (1) illustrates how minor changes in the biomolecule properties can result in significant variations in the term $1/C_s$.

Variations in dielectric properties of the biomolecular layer and the oxide layer cause changes in capacitance. These alterations lead to changes in the charge density across the junction, thus resulting in enhanced surface potential. As the dielectric constant (k) values increase, the electric field across the junction also increases, which leads to a higher degree of tunneling. Such tunneling effects significantly impact the electrical characteristics of biosensors, such as drain current (I_{DS}), subthreshold swing (SS), threshold voltage (V_{TH}), etc. Specifically, the increased sensitivity of the biosensor is an outcome of these changes in electrical characteristics.

An increase in the dielectric constant of biomolecules in the cavity region causes an increase in the electric field at the source–channel interface. Consequently, the width of the barrier is reduced, and the electron tunneling rate is increased. The effects of such variations on the electric field, energy band, and electron tunneling rate are clearly illustrated in Figs. 4(a)–4(c), respectively. On the other hand, figures 4(d)–4(f) illustrate the implications of charged biomolecules on device characteristics. Specifically, by increasing the negative (positive) charged densities of biomolecules, the electric field decreases (increases) at the tunneling junction. The net result of these effects is a decrease (increase) in the electron tunneling rate and, accordingly, a decrease (increase) in the device's ON-current. It is worth noting that the proposed biosensor exhibits greater drain current when there is an increase in the dielectric constant and a positive charge density of biomolecules.

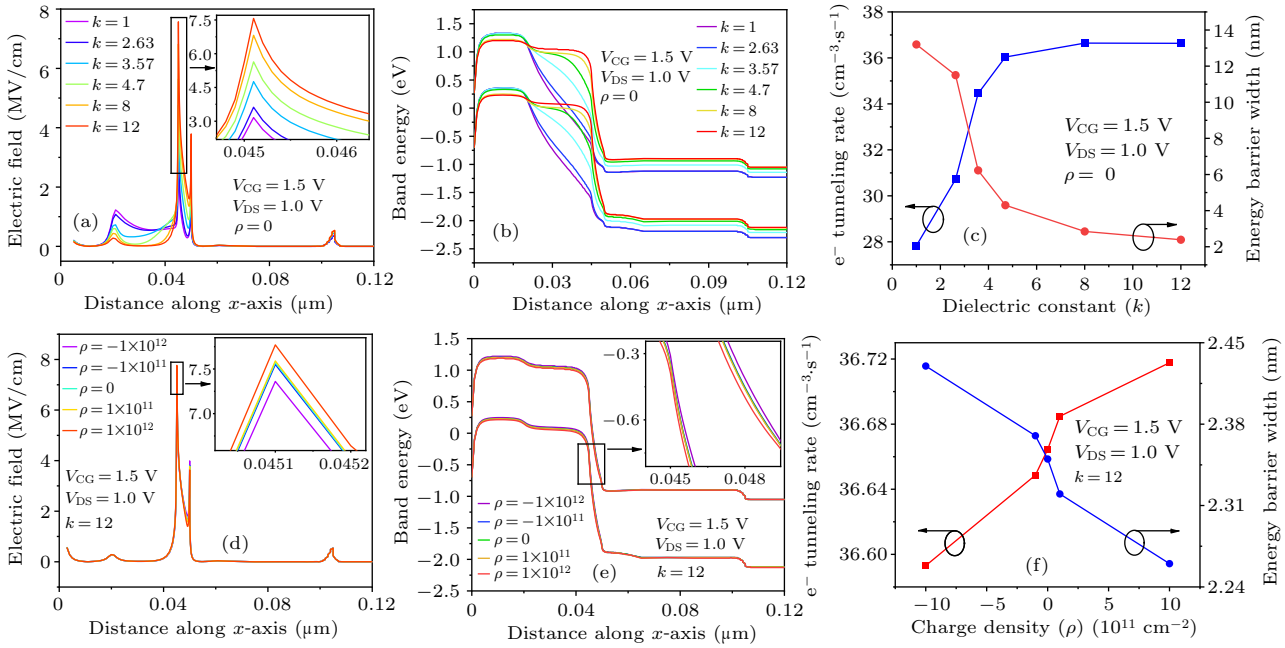


Fig. 4. Variation in (a) and (d) electric field, (b) and (e) band energy, (c) and (f) e^- tunneling rate and energy barrier width; (a)–(c) with different k at $\rho = 0$, (d)–(f) with different ρ at $k = 12$.

3.1. Sensitivity analysis

The biosensing applications require high sensitivity for detecting biomolecules, which is usually evaluated using measures such as drain current (I_{DS}), threshold voltage (V_{TH}), and subthreshold swing (SS). Achieving high sensitivity is desirable in such applications.

The I_{DS} sensitivity in the proposed in-built N^+ pocket ED-TFET biosensor is defined as the ratio of change in drain current when the cavity region is filled with the dielectric constant of biomolecules ($k > 1$) compared to when it is filled with air ($k = 1$), i.e., $S_{I_{DS}} = \Delta I_{DS}/I_{DS}^{(air)}$.[36] The sensitivity of the biosensor current increases with increasing dielectric constants of biomolecules in the nanocavity region, as shown in Fig. 5(a). The dependency of S_{IDS} on the dielectric constant is depicted in Fig. 5(c), which indicates that the sensitivity of the proposed biosensor to drain current increases as the k value increases. However, the $S_{I_{DS}}$ exhibits an initial rise followed by a decline as the CG voltage increases. This outcome is due to the transition of the TFET into an on state at a CG voltage of 1.15 V for $k = 1$, resulting in an increase in the drain current, which reduces the overall sensitivity to current. Therefore, the highest $S_{I_{DS}}$ of 1.08×10^{13} is achieved at a V_{CG} of 1.15 V for $k = 12$.

Moreover, figures 5(b) and 5(d) illustrate the variation of $S_{I_{DS}}$ with charged biomolecules. The biosensor's sensitivity to the drain current increases with increasing positive charge density due to the higher concentration of holes in the source region. However, the negatively charged biomolecules exhibit an opposite behavior because the number of holes in the source region decreases. Similar to the dielectric constant, the sensitivity of interface charge shows a trend of increase, followed by a decline with an increase in k value. The proposed biosensor provides $S_{I_{DS}}$ of 1.37×10^{13} with positively charged biomolecules at $\rho = +1\times10^{12}$ cm^{-2} ($k = 12$), while it provides $S_{I_{DS}}$ of 8.58×10^{12} with negatively charged biomolecules at $\rho = -1\times10^{12}$ cm^{-2} ($k = 12$).

The impact of variations in dielectric constant and charge density on SS and subthreshold swing sensitivity (S_{SS}) of the proposed biosensor has been thoroughly examined. The S_{SS} of in-built N^+ pocket ED-TFET biosensor is evaluated as follows:[37]

$$S_{SS} = \left(\frac{SS_{(air)} - SS_{(bio)}}{SS_{(air)}}\right). \tag{2}$$

As depicted in Fig. 6(a), the SS of in-built N^+ pocket ED-TFET biosensor decreases as the dielectric constant of neutral biomolecules increases, while the SS sensitivity shows an increase. Additionally, figure 6(b) presents the effect of charged biomolecules on the SS sensitivity of the biosensor. Here, it can be observed that as the concentration of interface charge increases, the SS decreases, which is accompanied by a rise in SS sensitivity.

Figures 6(c) and 6(d) illustrate the threshold voltage and its sensitivity of the proposed biosensor in relation to the dielectric constant and charge density. The threshold voltage sensitivity (S_{VTH}) is defined as follows:[38]

$$S_{V_{TH}} = \left(\frac{V_{TH}^{(air)} - V_{TH}^{(bio)}}{V_{TH}^{(air)}}\right). \tag{3}$$

The results shown in Figs. 6(c) and 6(d) indicate that S_{VTH} increases as the k value rises, whereas it decreases with increasing charge density.

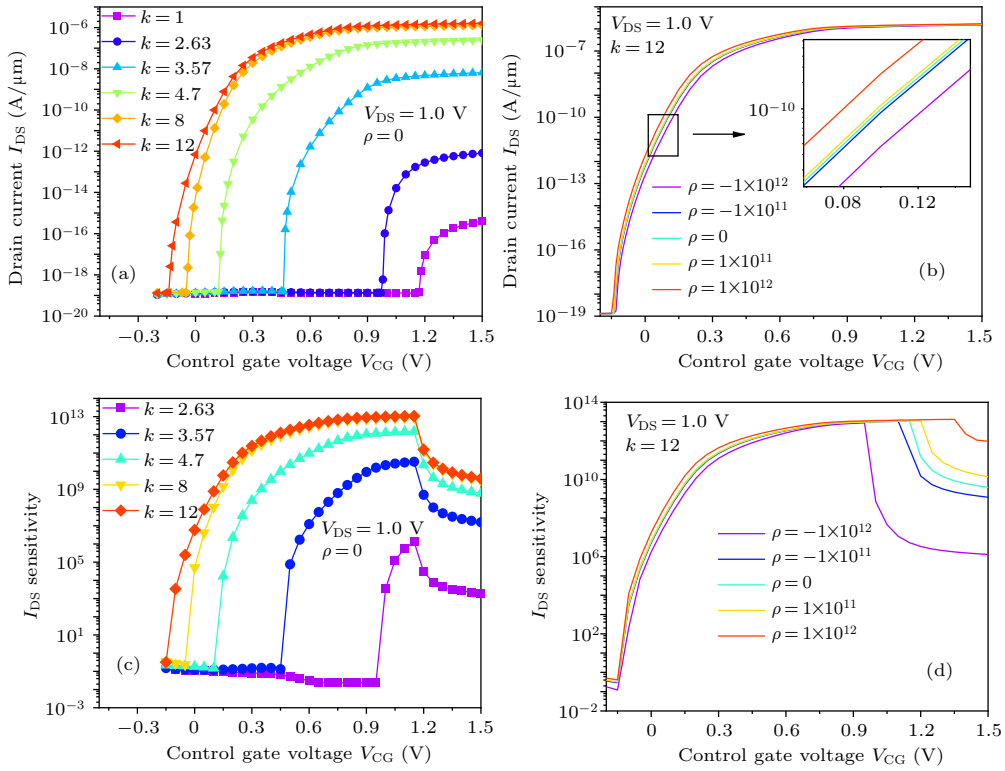


Fig. 5. I_{DS}–V_{CG} plot of the in-built N^+ pocket ED-TFET biosensor with varying (a) k at $\rho = 0$ and (b) ρ at $k = 12$. I_{DS} sensitivity along V_{CG} with different (c) k at $\rho = 0$ and (d) ρ at $k = 12$.

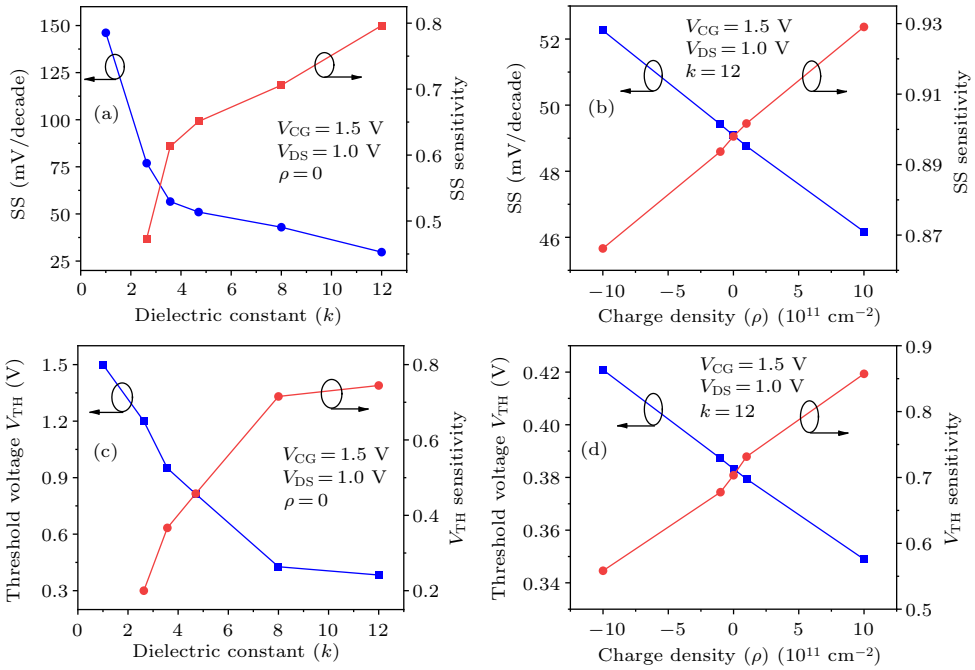


Fig. 6. SS and SS sensitivity variations with varying (a) k at $\rho = 0$ and (b) ρ at $k = 12$. Threshold voltage and threshold voltage sensitivity variations with various (c) k at $\rho = 0$ and (d) ρ at $k = 12$.

The I_{ON}/I_{OFF} ratio is a crucial characteristic of nanoscale devices, and thus, the sensitivity of the proposed biosensor can be evaluated in terms of this ratio, calculated using the following equation:[39]

$$S_{I_{ON}/I_{OFF}} = \left(\frac{(I_{ON}/I_{OFF})^{bio} - (I_{ON}/I_{OFF})^{air}}{(I_{ON}/I_{OFF})^{air}} \right). \quad (4)$$

As the dielectric constant of the biomolecules in the cavity region increases, the barrier width at the tunneling junction decreases. This leads to an enhanced tunneling rate and an increase in the ON current, thereby improving the I_{ON}/I_{OFF} sensitivity. This effect is depicted in Fig. 7(a). Additionally, an increase in the positive (negative) charge density of biomolecules results in a higher hole concentration (electron concentration) in the source region, leading to an increase (decrease) in the drain current. Consequently, the I_{ON}/I_{OFF} sensitivity increases (decreases), as illustrated in Fig. 7(b).

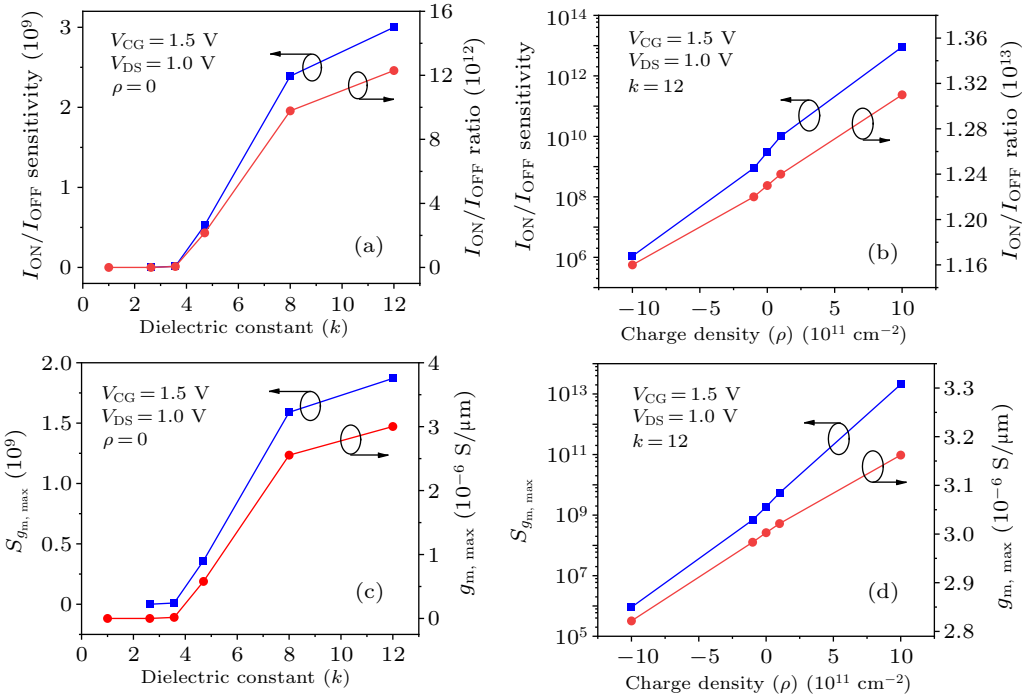


Fig. 7. I_{ON}/I_{OFF} sensitivity and I_{ON}/I_{OFF} ratio variations with different (a) k at $\rho = 0$ and (b) ρ at $k = 12$; $g_{m,max}$ sensitivity and $g_{m,max}$ variations with different (c) k at $\rho = 0$ and (b) ρ at $k = 12$.

The next parameter evaluated in this paper is $S_{g_{m,max}}$, defined by the following equation:[40]

$$S_{g_{m,max}} = \frac{g_{m,max}^{(bio)} - g_{m,max}^{(air)}}{g_{m,max}^{(air)}}, \tag{5}$$

where $g_{m,max}^{(bio)}$ represents the maximum transconductance of the device when the nano-detection cavity is filled with materials possessing varying dielectric constants, and $g_{m,max}^{(air)}$ corresponds to $g_{m,max}$ when the nano-detection cavity is unfilled. As illustrated in Fig. 7(c), both $g_{m,max}$ and $S_{g_{m,max}}$ are observed to increase progressively with higher k values. Additionally, figure 7(d) demonstrates that as the interface charge density rises, both $g_{m,max}$ and $S_{g_{m,max}}$ also exhibit a gradual increase.

3.2. Considering of non-ideal issues

All the analyses conducted for the proposed biosensor so far have been predicated on the assumption of fully filled nano-cavities with biomolecules. However, in practical scenarios, it is unlikely for nano-cavities to be completely filled. When the cavities are only partially filled, the sensitivity of the biosensor tends to decrease. Therefore, it is essential to investigate the fill-factor (FF)-based sensitivity of the proposed biosensor to better understand the operational challenges it faces. The fill factor is defined as follows:[41]

$$\text{FF}\% = \left(\frac{A_{bio}}{A_{total}}\right) \times 100. \tag{6}$$

Here, A_{bio} denotes the area of the nanocavity occupied by biomolecules, while A_{total} represents the total area of the nanocavity. Figure 8(a) illustrates various levels of biomolecule accumulation at 25%, 50%, 75%, and 100%. Figure 8(b) presents a plot of current sensitivity against the fill factor for different k values. It is evident that increasing both the FF and the k values of the biomolecules leads to an enhancement in the sensitivity of the proposed biosensor. This enhancement occurs due to the capacitive coupling between the PG1 terminal and the source region increases, leading to greater sensitivity of I_{DS} with an improved FF. In conclusion, the fill factor plays a crucial role in influencing the sensitivity of the in-built N^+ pocket ED-TFET-based biosensor.

3.3. Effect of cavity geometry on sensitivity

In this work, we also investigated the effects of cavity geometry on the sensitivity of the proposed biosensor by modifying the cavity lengths (L_{cavity}) and thicknesses (T_{cavity}). Figure 8(c) illustrates the variation in I_{DS} sensitivity with respect to cavity length. We simulated devices with cavity lengths of 20 nm, 25 nm, 30 nm, and 35 nm. As the cavity length increases, the capacitor area expands, enhancing the cavity's ability to control I_{DS}. Consequently, the sensitivity of the proposed biosensor improves with longer cavity lengths.

Moreover, we modified the cavity thickness of 13 nm, 15 nm, 17 nm, and 19 nm. The results show that as the cavity thickness increases, the current sensitivity decreases, as illustrated in Fig. 8(d). An increase in cavity thickness results in a reduction of the coupling capacitance between the source region and the PG1 terminal. Consequently, the influence of the PG1 terminal on the carrier concentration in the source region diminishes. This decline in control leads to less band bending at the tunneling interface, which in turn lowers both I_{DS} and I_{DS} sensitivity.

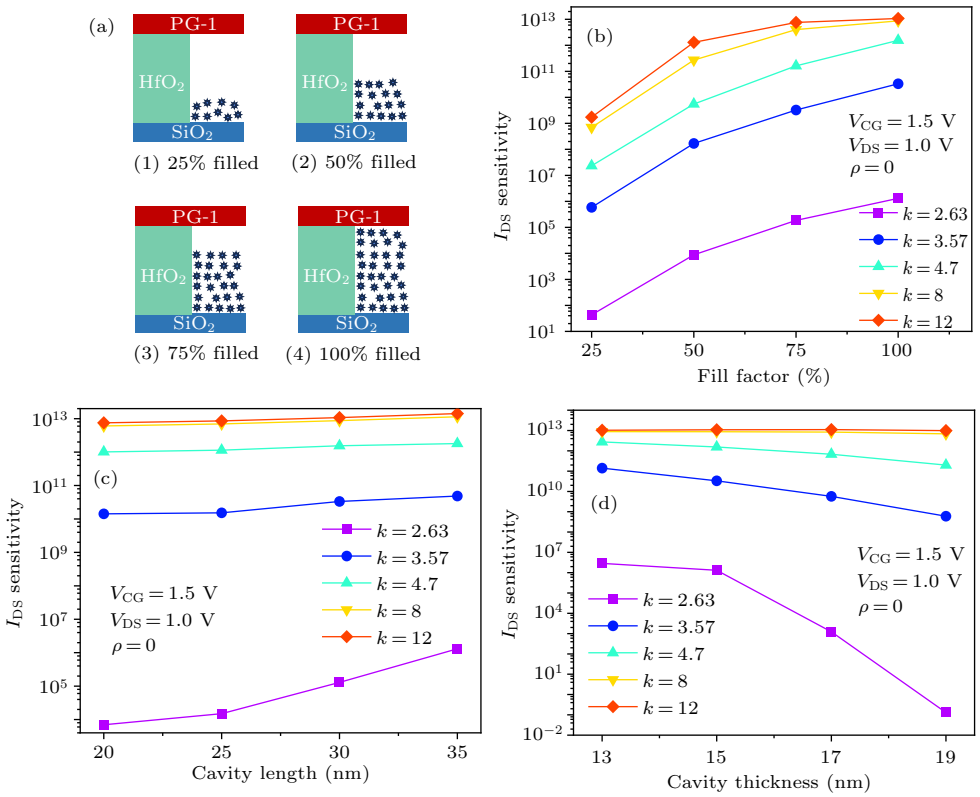


Fig. 8. (a) Nanocavity filled with different FFs and (b) I_{DS} sensitivity along varying FFs at different k. Variation in current sensitivity of the in-built N^+ pocket ED-TFET biosensor with different (c) cavity lengths and (d) cavity thicknesses.

3.4. Effect of thermal drift on sensitivity considering of non-ideal issues

The electrical parameters of semiconductor devices are generally sensitive to variations in temperature, making it crucial to assess the impact of temperature changes on the sensitivity of the proposed biosensor. In our simulations, we analyzed the device performance at temperatures of 280 K, 300 K, and 320 K.

As illustrated in Fig. 9(a), the drain current of the proposed biosensor increases and V_{TH} shifts to the left with rising temperature. However, it is evident that the I_{DS} and V_{TH} are not significantly affected by temperature variations because the proposed device operates based on the band-to-band tunneling mechanism. This means that the current in this device relies more on tunneling phenomena rather than directly on thermal effects. Despite the increase in I_{DS} with temperature, the sensitivity of the biosensor experiences a decrease, as shown in Fig. 9(b). This phenomenon can be interpreted through two competing effects that occur when the nano-cavities are filled with biomolecules. First, as temperature increases, the tunneling barrier width decreases, which leads to an increase in I_{DS}. Second, the dielectric constant of the immobilized biomolecules decreases with rising temperature, causing a reduction in capacitive between the polarity gate terminal (PG1) and the source region. The latter effect negatively impacts the current sensitivity.

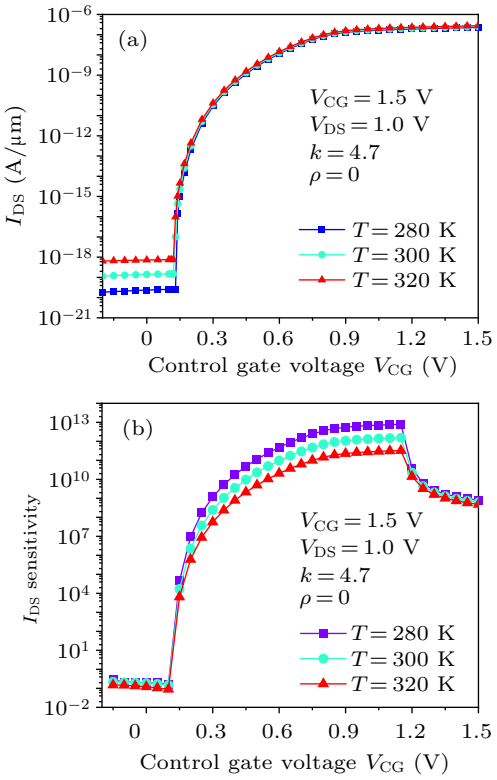


Fig. 9. (a) I_{DS}–V_{CG} characteristics and (b) I_{DS} sensitivity at different temperatures (280 K, 300 K, and 320 K).

Consequently, while I_{DS} increasing due to the narrowing of the tunneling barrier when the nano-cavity is empty, this increase is offset by the decrease in sensitivity when the cavity is filled with biomolecules. Therefore, we can conclude that the

sensitivity of the proposed biosensor decreases with increasing temperature, primarily due to the dual impact of increased I_{DS} in empty cavities and reduced capacitive coupling in filled cavities as ambient temperature rises.

3.5. Selectivity analysis

A fundamental attribute of biosensors is their selectivity, which refers to the ability to differentiate between target biomolecules and other biomolecules present in the nanocavities. According to Eq. (7), selectivity can be quantitatively assessed by measuring the variance in drain current between the target biomolecules and the reference biomolecules.

$$\Delta S = \left(\frac{I_{\text{Target}}^{(\text{bio})} - I_{\text{Ref.}}^{(\text{bio})}}{I_{\text{Ref.}}^{(\text{bio})}} \right). \tag{7}$$

Here, $I_{\text{Target}}^{(\text{bio})}$ and $I_{\text{Ref.}}^{(\text{bio})}$ denote the drain currents obtained from the proposed biosensor when detecting the target biomolecules and reference biomolecules, respectively. To quantitatively evaluate this parameter, selectivity calculations were conducted for three different pairs of biomolecules: Ferrocytochrome c-APTES, Ferrocytochrome c-Biotin, and Keratin–Biotin. Figure 10 illustrates the selectivity of the proposed in-built N^+ pocket ED-TFET biosensor for various target biomolecules in relation to different reference biomolecules.

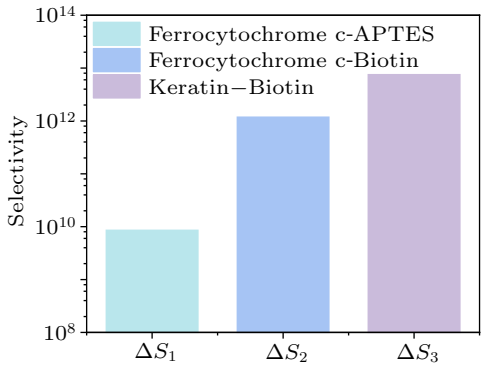


Fig. 10. Selectivity of the proposed biosensor between different pairs of biomolecules.

The results indicate that the highest selectivity, measured at 7.53×10^{12}, is attained by the biosensor for the Keratin–Biotin. This enhanced performance is largely attributed to the significantly larger value of $\Delta\varepsilon_k/\varepsilon_k$ observed for these specific biomolecules compared to other combinations.

In Table 3, we present a comparison of the current sensitivity of the proposed in-built N^+ pocket ED-TFET biosensors with previously reported tunnel TFET-based biosensors. The data indicate that the proposed biosensor exhibits superior sensitivity due to its innovative structural design, which incorporates a cavity and an in-built N^+ pocket on the source side. This unique configuration enhances the capacitive coupling and enables more effective molecular detection compared to other biosensors in the literature.

Table 3. Comparision of the in-built N^+ pocket ED-TFET biosensor performance parameters with published works.

References/ Year	Cavity dimensions	Dielectric constant (k)	Drain current sensitivity (approximate $S_{I_{DS}}$)
[26]/2024	$V_{GS}=1.0$ V,	3.57	1.95×10^{7}
	$V_{DS}=0.5$ V,	8	1.64×10^{10}
	$L_{cavity}=25$ nm,	12	1.34×10^{11}
	$T_{cavity}=5.5$ nm		
[30]/2024	$V_{GS}=2.0$ V,	4	8.0×10
	$V_{DS}=1.0$ V,	8	5.0×10^{4}
	$L_{cavity}=7$ nm,	12	3.68×10^{5}
	$T_{cavity}=5$ nm		
[38]/2024	$V_{GS}=1.2$ V,	4.7	2.0×10^{7}
	$V_{DS}=1.0$ V,	10	8.16×10^{9}
	$L_{cavity}=25$ nm,	12	5.30×10^{10}
	$T_{cavity}=15$ nm		
[41]/2024	$V_{GS}=3.0$ V,	7	3.0×10
	$V_{DS}=1.0$ V,	12	7.0×10^{2}
	$L_{cavity}=30$ nm,	22	8.61×10^{4}
	$T_{cavity}=3$ nm		
[42]/2022	$V_{GS}=0.4$ V,	2.63	6.0×10^{4}
	$V_{DS}=0.4$ V,	3.57	7.0×10^{5}
	$L_{cavity}=50$ nm,	8	6.17×10^{5}
	$T_{cavity}=7$ nm		
[43]/2024	$V_{GS}=1.5$ V,	8.7	5.8×10^{8}
	$V_{DS}=0.5$ V,	24.5	7.6×10^{9}
	$L_{cavity}=25$ nm,	32	2.7×10^{10}
	$T_{cavity}=2$ nm		
[44]/2025	$V_{GS}=2.0$ V,	4.5	2.0×10^{6}
	$V_{DS}=1.0$ V,	24.5	6.0×10^{8}
	$L_{cavity}=11$ nm,	32	9.05×10^{8}
	$T_{cavity}=5$ nm		
This work	$V_{GS}=1.5$ V,	2.63	1.31×10^{6}
	$V_{DS}=1.0$ V,	8	8.74×10^{12}
	$L_{cavity}=25$ nm,	12	1.08×10^{13}
	$T_{cavity}=15$ nm		

4. Conclusions and perspectives

In this article, we investigated the performance of the proposed in-built N^+ pocket ED-TFET biosensors for the label-free detection of both neutral and charged biomolecules. The analysis reveals that the sensitivity of the proposed N^+ pocket ED-TFET biosensors enhances with higher k-values and increased density of positively charged biomolecules, whereas it diminishes with a greater presence of negatively charged biomolecules. When assessing neutral biomolecules, the biosensor achieves a peak I_{DS} sensitivity of 1.08×10^{13}, a V_{TH} sensitivity of 0.74, an SS sensitivity of 0.80, and an I_{ON}/I_{OFF} sensitivity of 3×10^{9} with nanogaps fully filled at $k=12$. For biomolecules that are negatively charged, the maximum I_{DS} sensitivity recorded is 8.58×10^{12}, while for positively charged biomolecules, it is 1.37×10^{13}. The V_{TH} sensitivity for negatively charged molecules is 0.56, compared to 0.86 for positively charged ones. Similarly, the SS sensitivity is 0.87 for negatively charged biomolecules and 0.93 for positively charged. The I_{ON}/I_{OFF} sensitivities are 1.1×10^{6} for negatively charged and 9.07×10^{12} for positively charged biomolecules, with a charge density of -1×10^{12} C$\cdot$ cm^{-2} for negatives and 1×10^{12} C$\cdot$ cm^{-2} for positives, both at $k=12$. The increased sensitivity underscores its ability to detect lower concentrations of target biomolecules, which is critical for enhancing the reliability and accuracy of biosensing technologies. Overall, the simulation results highlight the advantages

of the in-built N^+ pocket ED-TFET design, demonstrating its potential for high-performance biosensing applications.

Acknowledgement

Project supported by the Ministry of Education's Supply and Demand Matching Employment and Education Project (Grant No. 2024110776329).

References

[1] Gao A, Lu N, Wang W and Li T 2016 *Sci. Rep.* **6** 225546
[2] Im H, Huang X, Gu B and Choi Y 2007 *Nat. Nanotechnol.* **2** 430
[3] Reddy N N and Panda D K 2021 *Silicon* **13** 3085
[4] Hemaja V and Panda D K 2022 *Silicon* **4** 1873
[5] Tayal S, Majumdar B, Bhattacharya S and Kanungo S 2023 *IEEE Trans. NanoBiosci.* **22** 174
[6] Bhalla N, Pan Y, Yang Z and Payam A F 2020 *ACS Nano* **4** 7783
[7] Bitra J and Komanapalli G 2023 *Sensing and Imaging* **24** 28
[8] Wangkheirakpam V D and Bhowmick B and Pukhrambam P D 2020 *IEEE Trans. Nanotechnol.* **19** 156
[9] Devi W V, Bhowmick B and Pukhrambam P D 2020 *IEEE Trans. Electron Dev.* **67** 2133
[10] Bitra J and Komanapalli G 2023 *IEEE Trans. Elect. Electron. Mater.* **24** 365
[11] Das D and Pandey C K 2024 *Micro Nanostruct.* **190** 207825
[12] Pathakamuri A K, Pandey C K and Ghosh P 2024 *Microsyst. Technol.*
[13] Ashok T and Pandey C K 2024 *Microelectron. J.* **144** 106071
[14] Gorla K and Pandey C K 2024 *Aeu-int J. Electron C* **177** 155229
[15] Gorla K and Pandey C K 2025 *Micro Nanostruct.* **198** 208060
[16] Nagavarapu V, Jhaveri R and Woo J C S 2008 *IEEE Trans. Electron Dev.* **55** 1013
[17] Cao W, Yao C J, Jiao G F, Huang D, Yu H Y and Li M F 2011 *IEEE Trans. Electron Dev.* **58** 2122
[18] Li J, Liu Y, Wei S F and Shan C 2020 *Micromachines* **11** 960
[19] Lahgere A, Sahu C and Singh J 2015 *IEEE Trans. Electron Dev.* **62** 2404
[20] Tirkey S, Sharma D, Yadav D S and Yadav S 2017 *IEEE Trans. Electron Dev.* **64** 3943
[21] Abdi D B and Kumar M J 2014 *IEEE Electron Dev. Lett.* **35** 1170
[22] Colloc'h N, Hajji M, Bachet B, L'Hermite G, Schiltz M, Prangé T, Castro B and Mornon J P 1997 *Nat. Struct. Mol. Biol.* **4** 947
[23] Kuzuya A, Numajiri K, Kimura M and Komiyama M 2008 *Nucleic Acids Symp. Ser.* **52** 681
[24] Kim S, Baek D, Kim J Y, Choi S J, Seol M L and Choi Y K 2012 *Appl. Phys. Lett.* **101** 073703
[25] Acharya B and Mishra G P 2020 *IEEE Sensor. J.* **20** 13969
[26] Nigam K K, Yadav P and Tikkiwal V A 2024 *Micro Nanostruct.* **191** 207844
[27] Anvarifard M K, Ramezani Z, Amiri I S and Nejad A M 2020 *Mater. Sci. Semicond. Process* **107** 104849
[28] Ramezani Z and Orouji A A 2017 *J. Electron. Mater.* **46** 2269
[29] Marchi M, Sacchetto D, Frache S, Zhang J, Gaillardon P E, Leblebici Y and De Micheli G 2012 2012 *IEDM Tech. Dig.* 8.4.1
[30] Kondavitee G S, Kumar R A and Karumuri S R 2025 *IEEE Sensor. J.* **25** 3444
[31] Min K S, Kang C Y, Park C, Park C S, Park B J, Park J B, Hussain M M, Lee J C, Lee B H, Kirsch P, Tseng H H, Jammy R and Yeom G Y 2009 *IEEE International Electron Devices Meeting* (IEDM), December 07–09, 2009, Baltimore, MD, USA, p. 1
[32] Silvaco Inc. 2018 *ATLAS User's Manual* (Santa Clara, CA: Silvaco Inc.) http://www.silvaco.com
[33] Omura Y, Horiguchi S, Tabe M and Kishi K 1993 *IEEE Electron Dev. Lett.* **14** 569
[34] Wang P F, Hilsenbeck K, Nirschl Th, Oswald M, Stepper Ch, Weis M, Schmitt-Landsiedel D and Hansch W 2004 *Solid-State Electron.* **48** 2281
[35] Venkatesh P, Nigam K, Pandey S, Sharma D and Kondekar P N 2017 *Superlattices Microstruct.* **109** 470
[36] Singh Km S, Kumar S and Nigam K 2021 *IEEE Trans. Electron Dev.* **68** 5784
[37] Iqbal M Y, Alam M S, Anand S and Amin S I 2022 *IEEE Trans. Nanotechnol.* **21** 251
[38] Gedam A, Acharya B and Mishra G P 2021 *IEEE Sensor. J.* **21** 16761
[39] Bind M K and Nigam K K 2024 *IEEE Sensor. J.* **24** 24023
[40] Jia H, Zhao L and Su Q 2024 *Micro Nanostruct.* **194** 207931
[41] Mahoodi M and Hosseini S E 2025 *Aeu-int J. Electron C* **188** 155568
[42] Kumar R A, Kondavitee G S, Wadhwa G and Karumuri S R 2024 *IEEE Sensor. J.* **24** 37923
[43] Cherik I C and Mohammadi S 2022 *IEEE Sensor. J.* **22** 10308
[44] Harika P, Kondavitee G S and Karumuri S R 2025 *IEEE Trans. NanoBiosci.* **24** 25